Four-wave mixing and phase conjugation in plasmas using ionization nonlinearities

John F. Federici* and Ernest J. Valeo
Princeton Plasma Physics Laboratory, Princeton, New Jersey, 08543
(Received 29 May 1990; revised manuscript received 29 April 1991)

Four-wave mixing in plasmas using ponderomotive and thermal nonlinearities has been extensively studied. Plasmas have received considerable attention since they become more efficient four-wave-mixing and phase-conjugation media at longer wavelengths (far infrared, 10 μm, to radio wave, 10 m). In this paper, the prospect of using an ionization nonlinearity in weakly ionized plasmas for degenerate four-wave mixing and phase conjugation is discussed. Like the thermal pressure nonlinearity, the ionization nonlinearity results from the heating of the plasma by the beat wave. However, as the local temperature increases, more neutral species are ionized by electron-impact ionization to form a beat-wave grating structure; instead of pushing the electrons into a grating structure (as with the thermal and ponderomotive nonlinearities), the electron density grating is created directly by ionization. Numerical estimates of the phase-conjugate reflectivity indicate reflectivities in the range of 10^{-4}–10^{-3} are possible in a weakly ionized steady-state gas-discharge plasma. The reflectivity is limited to this range due to the onset of an ionization instability (striations). Larger reflectivities may be possible for pulsed plasma sources.

PACS number(s): 52.40.Nk, 42.65.Hw, 42.65.Ma

I. INTRODUCTION

Recently, four-wave mixing (FWM) in plasmas using ponderomotive and thermal nonlinearities has been extensively studied [1–8]. Plasmas have received considerable attention since they become more efficient four-wave mixing and phase conjugation media at longer wavelengths (far infrared, 10 μm to radio wave 10 m). Phase conjugation (PC) may be simply defined as a process which reflects an incident light wave in a time-reversed manner [9, 10]. Four-wave mixing is one possible method of phase conjugation. Although FWM, using various nonlinear media, has many practical applications in the visible to infrared region of the electromagnetic spectrum (e.g., dispersion compensation, cavity resonators, and image processing), viable nonlinear media for FWM at wavelengths longer than 10 μm have not been fully developed. (Artificial Kerr mediums (AKM) are another possible long-wavelength (1 cm) optical medium [11–14]. However, typical response times of AKM are slow ($\sim$ 60 sec).) The major contribution of this paper is the identification and study of a new FWM mechanism in plasmas, the ionization nonlinearity, which may be exploited for long-wavelength FWM and phase-conjugation applications.

Physically, FWM in a plasma may be viewed as Bragg scattering of an electromagnetic (EM) wave from a plasma density modulation or grating. The low-frequency density modulation (beat-wave grating) is formed by the coupling (mixing) of two other electromagnetic waves via some plasma nonlinearity. An EM wave scatters from the density modulation grating to produce a scattered fourth EM wave.

Using the ponderomotive force as the plasma nonlinearity which couples EM waves in the plasma, Steel and Lam [1] first suggested collisionless plasmas as a viable degenerate four-wave mixing (DFWM) and PC medium for the infrared to microwave wavelength regime. Several authors [15, 5, 16, 17] have derived the four-wave mixing plasma response utilizing a collisionless fluid or Vlasov description of the plasma. Recent experiments [16] have demonstrated FWM and resonant FWM in collisionless plasmas.

For collisional plasmas, where the collisional absorption of the electromagnetic waves is small and the collisional mean-free path is shorter than the nonlinear density grating scale length (beat-wave wavelength), Federici and Mansfield [3, 4] have demonstrated that collisional heating generates a thermal force which substantially enhances the phase conjugate reflectivity over the ponderomotive value. DFWM and PC using thermal nonlinearity has recently been demonstrated using 10.6-μm light [6].

In this paper, the prospect of using a novel ionization nonlinearity in weakly ionized plasmas for degenerate four-wave mixing and phase conjugation is discussed. Like the thermal pressure nonlinearity [3, 4], the ionization nonlinearity results from the heating of the plasma by the beat wave. However, as the local temperature increases, more neutral species are ionized by electron-impact ionization to form a beat-wave grating structure; instead of pushing the electrons into a grating structure (as with the thermal and ponderomotive nonlinearities), the electron density grating is created directly by ionization.

For simplicity, our theory assumes that the dominant ionization-recombination processes are electron-impact ionization, three-body recombination, and recombination at the plasma boundary. Photoionization processes are neglected. Certainly, there are plasma parameter regimes (i.e., the ionospheric plasma, or high-density laser produced plasmas) where other processes, such as photoionization, might become important. The plasma conditions considered in this paper are similar to those found in steady-state gas-discharge plasmas [18, 19]. We

focus on this parameter regime since steady-state discharge plasmas can exhibit ionization instabilities or "striations" whose mechanism is analogous to the ionization nonlinearity of FWM. One would expect, therefore, that these plasmas would exhibit a strong ionization nonlinearity. As will be discussed later in Sec. V, steady-state discharges might not be the optimum plasmas for high phase-conjugate reflectivity in all parameter regimes. However, these plasmas serve as an example of the physics of the ionization nonlinearity.

The theory presented here applies to DFWM using electromagnetic wavelengths ranging from 10 μm to 1 cm. The corresponding electron density range is 10^{13} to 10^{17} cm^{-3} with typical electron temperatures of 1 eV. The fraction of ionization typically falls in the 1–10% range. Numerical estimates of the phase conjugate reflectivity indicate reflectivities in the range of 10^{-4}–10^{-3} are possible in a weakly ionized steady-state gas-discharge plasma. The reflectivity is limited to this range due to the onset of an ionization instability (striations). Larger reflectivities may be possible for pulsed plasma sources.

A. Simple derivation of $\chi^{(3)}$

In Secs. III and IV, a detailed derivation of the four-wave-mixing plasma response, which utilizes an asymptotic expansion for the nonlinear polarizability, nonlinear current density, and plasma fluid variables, in powers of the electromagnetic electric field amplitude, is presented. In this section, a simplified derivation of $\chi^{(3)}$ for ionization nonlinearities is discussed.

The coupling of the electromagnetic waves in four-wave mixing can be described via a nonlinear polarizability of the medium. For plasmas, the nonlinear polarization may also be interpreted as a nonlinear current since $\partial P/\partial t \simeq J$. Generically, the nonlinear polarization of a medium may be written as [9, 10]

$$P_i = \chi^{(1)}_{ij} E_j + \chi^{(2)}_{ijk} E_j E_k + \chi^{(3)}_{ijkl} E_j E_k E_l + \cdots, \quad (1)$$

where summation over repeated indices is implied, E_i represents the ith electric-field component of the total *electromagnetic* field ($\nabla \cdot \mathbf{E} = 0$; no electrostatic wave), and $\mathbf{P}$ represents the EM polarizability of the medium. The *order* of the nonlinearity is determined by the factor of electric-field amplitudes. This convention of counting EM amplitudes is different from other conventions where the order of the interaction is defined by the number of normal modes, including electrostatic modes (eg., plasma wave, sound waves), in the interaction. The $\chi^{(1)}_{ij}$ term of Eq. (1) enters the linear dispersion relation. The $\chi^{(2)}_{ijk}$ term represents second-order nonlinearities since it couples two EM amplitudes. The $\chi^{(2)}_{ijk}$ term is nonzero only in a material which lacks inversion symmetry [9], such as a crystal with a preferred direction or a *magnetized* plasma. The $\chi^{(3)}_{ijkl}$ term represents the coupling of three EM amplitudes.

In this paper, we are interested in the FWM components of the $\chi^{(3)}_{ijkl}$ matrix. However, we note that ionization nonlinearities may also play a role in other third-order nonlinearities such as self-focusing. As discussed in Sec. III and shown in Ref. [4], the dominant FWM components of $\chi^{(3)}$ may be calculated using the nonlinear current density $\mathbf{J}_3 = -en^e_2\mathbf{v}^e_1$ (since $\partial\mathbf{P}/\partial t \sim \mathbf{J}$), where $\mathbf{v}^e_1$ is the electron "quiver" velocity of an electron in an electromagnetic field and n^e_2 is the beat-wave electron density response analogous to the density grating of Bragg scattering. The nonlinear current represents the scattering of an EM wave from the Bragg grating to drive the fourth EM wave.

The general phase-matching conditions for four-wave mixing are

$$\mathbf{k}_p + \mathbf{k}_s = \mathbf{k}_f + \mathbf{k}_b, \quad \omega_p + \omega_s = \omega_f + \omega_b. \quad (2)$$

These relations may be simply understood as conservation of momentum and energy in the wave interaction. In the above expression, the forward pump, backward pump, probe, and scattered wave are denoted by subscripts f, b, p, s as in Fig. 1. (Occasionally, the subscript c is used in place of s to identify the "scattered" wave with the phase-conjugate wave.) In this paper, we consider the pump beams to be of comparable intensity. For unequal intensities, see Refs. [8, 20]. Moreover, we only consider the weak-signal regime (phase-conjugate reflectivity less than unity). All the electromagnetic frequencies are positive; the direction of wave propagation is given by the direction of the wave vector. For DFWM, the frequency-phase-matching condition is satisfied since all of the frequencies are identical. If the pump beams were antiparallel, then $\mathbf{k}_f + \mathbf{k}_b = 0$, $\mathbf{k}_s = -\mathbf{k}_p$, and a phase conjugate signal of the probe would be produced.

Consider a simple heuristic estimate of the ionization nonlinearity beat-wave electron density response for a weakly ionized plasma which is close to Saha equilibrium. In the plasma, electron-impact ionization of neutral atoms is assumed to nearly balance three-body recombination [21]. In this limit, the electron density has the form $n_e \simeq N_0 \exp(-I_0/T_0)$, where I_0 is the ionization potential of the neutral gas, T_0 is the electron temperature, and $I_0/T_0 \gg 1$. Using the beat wave of the probe wave and one of the pump waves to locally heat the plasma, the resultant density variation would be approximately

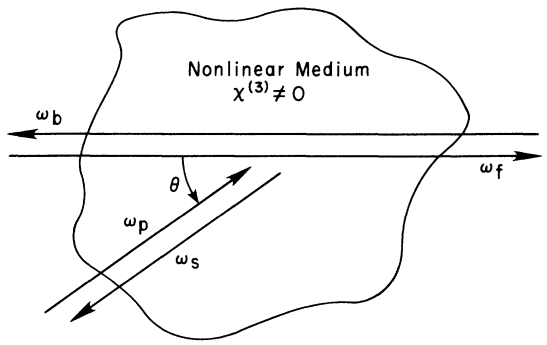

FIG. 1. Degenerate four-wave-mixing geometry. The subscripts f, b, p, s refer to the forward pump, backward pump, probe, and signal wave, respectively.

$$\frac{\delta n_e}{n_e} \simeq \frac{I_0}{T_0}\frac{\delta T_0}{T_0}.$$

The normalized density fluctuations are much larger than the temperature fluctuations due to the exponential temperature dependance. For the thermal pressure nonlinearity (Refs. [4, 3]), the corresponding balance between density and temperature is $\delta n_e/n_e \simeq -\delta T_0/T_0$ (due to the constant electron pressure $P_e = N_e T_0$). Consequently, ionization nonlinearities are stronger than thermal force nonlinearities by a factor of I_0/T_0.

Returning to the estimation of the ionization beat-wave amplitude, the temperature fluctuation amplitude is limited by the dominant energy-loss process. For typical situations discussed in this paper, electron thermal conduction is the dominant energy-loss mechanism so that the temperature fluctuation is determined from $Q_{\mathrm{BW}} \simeq \kappa^e \nabla^2 T_e$ to be

$$\frac{\delta T_e}{T_e} \simeq \frac{Q_{\mathrm{BW}}}{N_0 T_0}\frac{N_0}{\kappa^e k_{mn}^2}$$

where κ^e is the electron thermal conduction, Q_{BW} is the power deposited per unit volume in the plasma due to the beat-wave heating, and k_{mn} is the beat-wave wave number. The beat-wave heating has the form

$$Q_{\mathrm{BW}} \simeq m_e N_0(\nu_{ei} + \nu_{ea}) v_m^e v_p^e$$

where v_p^e (m) is the quiver velocity of an electron in the probe (pump) electric field, m_e is the electron mass, N_0 is the electron density, ν_{ei} (ν_{ea}) is the electron-ion (electron–neutral-species) collision frequency. The beat-wave amplitude is approximately

$$\frac{\delta n_e}{n_e} \simeq \frac{I_0}{T_0}\frac{Q_{\mathrm{BW}}}{N_0 T_0}\frac{N_0}{\kappa^e k_{mn}^2}.$$

As noted previously, this is a factor of I_0/T_0 larger than the thermal force nonlinearity.

The Bragg reflection coefficient may be approximated as [22]

$$R = \frac{I_s}{I_p} \simeq \left|\frac{2\pi\omega}{c}\chi^{(3)} E_f E_b\right|^2 L^2 \simeq \frac{E_f E_b}{E_p^2}\left(\frac{\pi \delta n_e\, N_0\, L}{2 N_0\, N_c\, \lambda}\right)^2,$$

where I_s (I_p) is the intensity of the scattered (probe) wave, E_f (b, p, s) is the magnitude of the forward pump electric field, L is the interaction length of the FWM process, ω is the EM frequency, c is the speed of light, λ is the EM wavelength, and N_c is the critical density at frequency ω. The FWM $\chi^{(3)}$ may be shown to be approximately

$$\chi^{(3)} \simeq \frac{e \delta n_e v_1^e}{\omega E_f E_b E_p}.$$

B. Analogy with semiconductors and striations

Semiconductors exhibit an analogous "ionization nonlinearity" for FWM [23]. In semiconductors, the coupled pump and probe waves generate a large concentration of free carriers (electron-hole plasma) by optically inducing transitions of electrons between the valance and conduction bands. For laser wavelengths near a semiconductor band gap, the electron-hole plasma is generated by single photon absorption [23–25]. For laser frequencies far from a band-gap resonance, the electron-hole plasma is generated by multiphoton absorption processes [26].

The major differences between ionization nonlinearities in semiconductors and in plasmas are the physical mechanisms for the generation of the plasma and the maintenance of the ionization balance. For long-wavelength (infrared to centimeter waves) phase conjugation in plasmas, neutral species are predominantly ionized by electron impact ionization rather than by photoionization. In principle, ionization mechanisms other than electron-impact may be important for plasmas. For example, multiphoton or single photon photoionization processes may become important if the EM field intensity is strong enough or if the photon energy is comparable to an ionization potential. This paper, however, will focus plasmas in which electron-impact ionization, three-body recombination, and wall recombination are the dominant processes. It is assumed that the electron-impact ionization rate is larger than the photoionization rate $(SN_a \gg \nu_{\mathrm{ph}})$.

The nonlinear mechanism which generates the ionization grating for FWM is similar to the mechanism for ionization instability-driven electron-density waves in gas-discharge plasmas. These waves are also called striations or ionization waves [19, 27, 18, 28, 29]. Striations exist in discharge plasmas under various plasma and discharge conditions [19]. The striations consist of layers of alternating high and low electron density. Striations may be either quasineutral [18] or space charge [19, 27, 28] waves depending on the current, type of gas, gas pressure, etc. Striations also may be produced in optical discharges [30–32] (commonly called laser sparks). The mechanism for "optical striations" is similar to the mechanism for discharge plasma striations. Not only are ionization waves and striations in plasmas of interest since their mechanism is similar to that of FWM, but they are also of interest since the formation of striations may affect the plasma equilibrium as discussed in Sec. V. In this paper, we focus on the plasma parameter regime which is typical for striations in gas discharges.

This paper is organized as follows: Section III describes the perturbative expansion which is used to calculate the four-wave mixing in the plasma. Section II describes the equilibrium conditions and fundamental parameters. Section III derives and solves the beat-wave equations for the electron density response. Estimated phase-conjugate reflectivities for typical plasma parameters are present in Sec. IV. The stability of the equilibrium plasma is discussed in Sec. V. Conclusions are presented in Sec. VI.

II. EQUILIBRIUM CONDITIONS AND STARTING EQUATIONS

Following the analogy of the ionization nonlinearity to the ionization instabilities in striations, we choose plasma

conditions and geometries which are typical for gas discharges. Consider a FWM geometry as in Fig. 2 for a partially ionized plasma. The boundaries denoted by the hash marks may be physical boundaries, such as a wall, or some other boundary, such as un-ionized gas. The plasma is assumed to be infinite in the $\hat{z}$ (or parallel) direction. The plasma is cylindrically symmetric with a radius a. A constant current J_0 in the $\hat{z}$ direction joule heats the plasma. The pump beams are counter propagating along the $\hat{z}$ axis with the probe intersecting the $\hat{z}$ axis at angle θ. Furthermore, the electromagnetic wavelength λ as well as the beat-wave wavelength are assumed to be small compared to the physical dimensions of the plasma ($ka = 2\pi a/\lambda \gg 1$ and $k_{mn}a \gg 1$). By virtue of $k_{mn}a \gg 1$, we may further assume that the EM waves interact near the center of the discharge, in a homogeneous portion of the plasma. In this region of the plasma, contributions of equilibrium radial gradients to the plasma beat-wave equations may be neglected.

For simplicity, the electron-impact ionization rate (SN_a) is assumed to be large compared to the photoionization rate ($SN_a \gg \nu_{\rm ph}$) so that multiphoton ionization may be ignored. The effects of radiative losses on the ionization and energy balance are also ignored [4]. The dominant ionization and recombination mechanisms are electron-impact ionization, three-body recombination, and wall recombination. This paper, therefore, only considers plasmas which are in Saha balance (i.e., a range of possible equilibrium electron densities for which radiative recombination is small). We may estimate the density and temperature ranges for which the radiative recombination rate [33] $\alpha_r N_i \simeq 2.7 \times 10^{-13} T_e^{-1/2} N_e \ \sec^{-1}$ is negligible compared to the electron-impact ionization rate SN_a [Eq. (28)] and the three-body recombination rate [34] $\beta N_e^2 \simeq 8.75 \times 10^{-23} T_e^{-9/2} \ \sec^{-1}$. The density and temperature inequalities are

$$5 \times 10^{12} (SN_a) T_e^{1/2} \gg N_e \gg 3.1 \times 10^{13} T_e^4. \qquad (3)$$

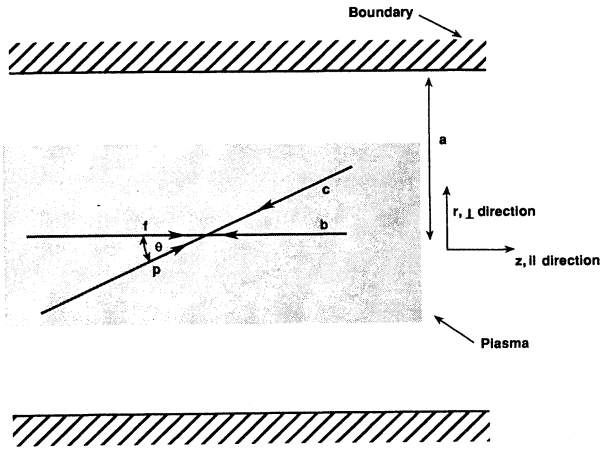

FIG. 2. FWM and plasma geometry for FWM in partially ionized plasma.

In equilibrium, all of the species are assumed to have the same temperature T_0. The equilibrium electron and ion densities are equal (N_0) and much smaller than the neutral atom density N_a. A necessary condition for $N_0/N_a \ll 1$ is that the ionization energy for the neutral species (I_0) be much larger than the plasma temperature ($I_0/T_0 \gg 1$). As a further simplification, the role of metastables in the ionization balance is ignored. Undoubtedly, there are many plasmas for which metastable neutrals would play a significant role [18, 28]. However, their potential roles in the ionization balance—such as in stepwise ionization—are beyond the scope of this paper.

The model fluid continuity and energy equations for the electrons', ions', and neutral species' equilibria and for their beat-wave responses are

$$\frac{\partial N_j}{\partial t} + \nabla \cdot (N_j \mathbf{v}_j) = G_j, \qquad (4)$$

$$\frac{3}{2} N_j \frac{dT_j}{dt} + P_j \nabla \cdot v_j = -\nabla \cdot q_j + Q_{\text{coll}\,j} + Q_{\text{laser}\,j} + \mathbf{J} \cdot \mathbf{E} - G_j I_0, \qquad (5)$$

where the subscript j refers to electrons, ions, or neutrals, and $N_j, \mathbf{v}_j, P_j$, and T_j are the fluid density, velocity, pressure, and temperature, respectively. $\mathbf{E}, \mathbf{q}_j, Q_{\text{laser}\,j}$, $Q_{\text{coll}\,j}$, $\mathbf{J} \cdot \mathbf{E}$, and G_j are the electric field, heat flux, laser, collisional, heat flux, laser, collisional, and joule heating terms, and rate of plasma plasma production due to ionization changes, respectively. The G term in the energy equation accounts for the changes in fluid energy due to ionization processes. The pressures are $P_j = N_j T_j$. The external heating term represents heating by the laser beams. In the equilibrium equations, this term represents bulk heating of the plasma by the laser beams, while in the beat-wave equations, it represents the laser heating on the beat-wave scale length. The ponderomotive term is not included in the momentum equation since thermal and ionization forces are expected to dominate in collisional plasmas.

Following the analogy with gas discharges, a generalized Ohm's Law [4] will be used to model the electron and ion momenta. The fundamental assumptions are that the collision frequencies are so large that the inertial terms in the momentum equations may be neglected and that the neutral velocity may be neglected compared to the electron velocity since momentum is transferred to the neu-

trals only through collisions (there are many more neutrals than electrons). The loss or gain in momentum as plasma is created or destroyed is neglected as described in Ref. [4]. As stated previously, it is assumed that the EM waves interact in the center of the plasma where equilibrium radial gradients are weak and can be ignored. Formally, the radial gradients are neglected since $k_{mn}a \gg 1$. The electron and ion momentum equations may be written in the form [4]

$$\mathbf{V}_e = -b_e\left(\mathbf{E} + \frac{\nabla(N_eT_e)}{eN_e}\right), \tag{6}$$

$$\mathbf{V}_i = b_i\left(\mathbf{E} - \frac{\nu_{ei}+\nu_{ea}}{\nu_{ea}}\frac{\nabla(N_iT_i)}{eN_e} - \frac{\nu_{ei}}{\nu_{ea}}\frac{\nabla(N_eT_e)}{eN_e}\right), \tag{7}$$

where $b_e \equiv e/m_e(\nu_{ei}+\nu_{ea})$ is the electron mobility, $b_i \equiv (e/m_i\nu_{ia})[\nu_{ea}/(\nu_{ei}+\nu_{ea})]$ is the ion mobility, $b_e \gg b_i$ by virtue of the mass ratio, and it is understood that the equilibrium radial components of the velocities and electric field have been eliminated (interaction in spatially homogenous region of plasma) and ∇ now refers to the gradients in the beat-wave (perturbed) quantities. The collision frequency for momentum exchange between electrons (ions) and neutrals is ν_{ea} (ν_{ia}). In the limit of $T_i \to 0$ and $\nu_{ei}/\nu_{ea} \to 0$, Eqs. (6) and (7) reduce to the Ohm's law equations which describe axial striations in a gas discharge [18].

The equilibrium equations are determined using Eqs. (4)–(7), and $\nabla_\perp(P_e+P_i+P_a)=0$ with $\partial/\partial t \to 0$ (equilibrium plasma stationary in time). The electrons and ions move together (ambipolar diffusion $\mathbf{v}_\perp^e = \mathbf{v}_\perp^i$) in the perpendicular direction (no perpendicular current). By symmetry, all of the equilibrium densities, velocities, etc., are independent of z.

For the purposes of this paper, the radial variations in the equilibrium profiles may be included in both the equilibrium and beat-wave equations using model terms. This practice is commonly followed in the literature on gas-discharge striations (See Ref. [18] and references therein. More detailed calculations of the radial profiles may be found in Refs. [35, 18]). Since the purpose of this paper is to study the basic physics of DFWM using ionization nonlinearities, model radial loss terms will be employed wherever applicable. With these simplifications, the equilibrium electron continuity equation becomes

$$\nabla_\perp(N_0^e\mathbf{V}_{0\perp}^e) = G_0 \equiv N_0^eN_0^aS - (N_0^e)^3\beta. \tag{8}$$

The electron continuity equation illustrates that any net production of plasma from electron-impact ionization and three-body recombination is balanced by particle flow to the boundary where the plasma recombines. There are two obvious limits of Eq. (8): When there is a local ionization balance (also termed "volume recombination" in the literature) electron-impact ionization and three-body recombination nearly balance each other ($N_eN_aS \simeq N_e^3\beta$). In the opposite limit, which is typically assumed for gas discharges, the diffusion/wall recombination term dominates three-body recombination. This paper will consider both regimes. However, as will be shown later, the wall-recombination plasma regime is not conducive to high phase-conjugate reflectivities.

The parallel equilibrium Ohm's law from Eqs. (6) and (7) is $\mathbf{J}_0 \equiv eN_0(\mathbf{V}_{i0}-\mathbf{V}_{e0}) = eN_0(b_e+b_i)\mathbf{E}_0$. The equilibrium electron energy equation is

$$P_e\nabla_\perp\cdot\mathbf{V}_e = -\nabla_\perp\cdot\mathbf{q}_e + \mathbf{J}_0\cdot\mathbf{E}_0 + Q_{0\,\text{laser}} + Q_{0\,\text{coll}} - GI_0. \tag{9}$$

The joule and laser heating predominantly heat the electrons, rather than the ions and neutrals, by virtue of the mass ratio. As discussed previously, in the interest of simplifying the analysis, we take the equilibrium equation to have the form

$$J_0E_0 + Q_{0\,\text{laser}} = N_eH, \tag{10}$$

where N_eH is the phenomenological energy-loss rate to the wall. In our model, the joule and laser heating are balanced predominantly by the heat loss to the boundary (which scales as $D_eN_0T_0/a^2$ where $D_e \equiv b_eT_0/eN_0$ is the electron diffusion coefficient).

The stability of the equilibrium is considered in Sec. V. For a steady-state gas discharge, as will be discussed later, stability considerations impose a maximum pump wave intensity which therefore limit the attainable reflectivities to the 10^{-4} range. However, high reflectivities may be possible in pulsed plasma sources.

The beat-wave response is determined by linearizing [36] Eqs. (4)–(7), and representing the beat-wave heating term as an external heating term. The perturbative expansion of the fluid equations and resulting beat-wave plasma response is considered in Sec. III.

III. PERTURBATIVE EXPANSION AND BEAT-WAVE EQUATIONS

Following the procedure outlined in Refs. [4] and [3], we calculate the coupling coefficient $\chi^{(3)}$ and the phase-conjugate reflectivity for the FWM interaction using a perturbative expansion for the fluid variables in powers of the electromagnetic field. By representing the pump, probe, and conjugate EM waves as

$$\mathbf{E}_1 = \tfrac{1}{2}[\,\mathbf{E}_n\exp(i\mathbf{k}_n\cdot\mathbf{r} - i\omega_nt) + \mathbf{E}_n^*\exp(-i\mathbf{k}_n^*\cdot\mathbf{r} + i\omega_nt)],$$

where $*$ denotes complex conjugate, it may be shown that in an isotropic medium (e.g., an unmagnetized plasma) the phenomenological form of the conjugate wave's FWM nonlinear polarizability is [10]

$$\mathbf{P}_c = \chi_{fp}^{(3)}(\mathbf{E}_f\cdot\mathbf{E}_p^*)\mathbf{E}_b + \chi_{bp}^{(3)}(\mathbf{E}_b\cdot\mathbf{E}_p^*)\mathbf{E}_f. \tag{11}$$

The $\chi^{(3)}$ nonlinearity is calculated using perturbation theory and expanding the polarizability Eqs. (1) and (11); or equivalently the current, in powers of the EM electric field. The polarizability is related to the nonlinear current by $\partial \mathbf{P}/\partial t = \mathbf{J}$. The dominant contribution to the nonlinear current may be shown to be $\mathbf{J}_3 = -en_2^e\mathbf{v}_1^e$ where n_2^e is the beat-wave electron density response and $\mathbf{v}_1^e$ is the electron "quiver" velocity $eE/m\omega$ in the EM wave [4].

In order to calculate the nonlinear current, two sets of fluid equations are required for the two distinct time scales: the fast electromagnetic time scale which gives v_1^e and the slow beat-wave time scale which gives n_2^e. The velocity and density responses v_1^e and n_2^e are calculated by perturbatively expanding the densities, velocities, electric field, etc. of the plasma fluid equations in powers of the EM electric field. All first-order terms oscillate on the EM time scale while the second-order terms evolve on the slow time scale:

$$\begin{aligned} N &= N_0 + n_1(k_n,\omega_n) + n_2(k_{mn},\omega_{mn}),\\ V &= 0 + V_1(k_n,\omega_n) + V_2(k_{mn},\omega_{mn}),\\ E &= 0 + E_1(k_n,\omega_n) + E_2(k_{mn},\omega_{mn}),\\ T &= T_0 + T_1(k_n,\omega_n) + T_2(k_{mn},\omega_{mn}), \end{aligned} \tag{12}$$

where $\omega_{mn} = \omega_m - \omega_n$, $\mathbf{k}_{mn} = \mathbf{k}_m - \mathbf{k}_n$ are the beat-wave frequency and wave number, respectively. In the expansion, $k_{mn}\lambda_{di}, k_{mn}\lambda_{mfp}$, and ν_e/ω_n (or equivalently $\lambda_n v_{te}/\lambda_{mfp}c$) are assumed to be small where λ_{di}, λ_{mfp}, and ν_{ei} are the ion Debye length, electron mean-free-path, and electron-ion collision frequency, respectively. The parameter $\nu_{ei}/\omega_m \ll 1$ implies that the collisional damping of the EM waves is weak. E_1 is the imposed laser beam electric field and E_2 is the self-consistent plasma electric field determined by ambipolar constraints. The zeroth-order density and temperature are assumed constant. The probe, pump, and signal electric fields are approximated as plane waves

$$\mathbf{E}_1 = \tfrac{1}{2}[\mathbf{E}_{1n}\exp(i\mathbf{k}_n\cdot\mathbf{r} - i\omega_n t) + \mathbf{E}_{1n}^*\exp(-i\mathbf{k}_n^*\cdot\mathbf{r} + i\omega_n t)], \tag{13}$$

where $\mathbf{k}_n = \mathbf{k}_{r_n} + i\alpha\hat{\mathbf{k}}_{r_n}$, α is the absorption coefficient in Eq. (14), ω_n is the wave frequency (positive definite), $\mathbf{k}_n$ is the wave vector (choosing $\mathbf{k}$ defines the direction of propagation), and n refers to the forward pump, backward pump, or the probe wave. The effective collision frequency [37] and adsorption coefficient are approximately [4]

$$\alpha = \frac{\omega_{pe}^2\nu_{hf}}{2\omega^2 c}\left(1 - \frac{\omega_{pe}^2}{\omega^2}\right)^{-1/2}, \tag{14}$$

$$\nu_{hf} = \frac{\nu_{ei} + \nu_{ea}}{2}, \tag{15}$$

$$\nu_{ei} = \frac{4\sqrt{2\pi}N_e e^4 \ln\Lambda}{3\sqrt{m_e}(T_e)^{3/2}}, \tag{16}$$

where ν_{ea} is the electron-neutral collision frequency as defined in Sec. IV. In the above equations, T_e is in units of ergs and $\ln\Lambda$ is the Coulomb logarithm [38]. Furthermore, the frequency and wave vector of each of the electromagnetic waves satisfies the dispersion relation $\omega_n^2 = \omega_{pe}^2 + k_n^2c^2$.

A simple linearization of fluid equations [4,3] governing the EM oscillations for the electrons yields

$$\mathbf{v}_1^e = \frac{1}{2}\mathbf{v}_{1n}^e\exp(i\mathbf{k}_n\cdot\mathbf{x} - i\omega_n t) + \text{c.c.} \tag{17}$$

$$\mathbf{v}_{1n}^e = \frac{-ie\mathbf{E}_{1n}}{m_e\omega_n} \tag{18}$$

where $\mathbf{v}_{1n}^e$ is the well-known quiver velocity of an electron in an EM field.

The low-frequency, second-order electron density beat-wave response n_2^e is calculated from the linearization of Eqs. (4)–(7). However, the equations for the beat-wave response of the plasma are significantly simplified by using phenomenological radial loss terms in the continuity and energy equations as well as exploiting $1/(k_{mn}a) \ll 1$ where a is the radius of the plasma. (One scenario which is being ignored here is FWM in a waveguide. In a waveguide, the electromagnetic wavelength is comparable to the waveguide dimension.)

The radial loss term is particularly useful in the continuity equation [Eq.(4)]:

$$N_0\tilde{z} = \frac{\partial n_e}{\partial t} + \nabla\cdot(n_e\mathbf{v}_e), \tag{19}$$

$$\tilde{z} \equiv SN_a - \beta N_0^2 - D_a/a^2, \tag{20}$$

where $D_a \equiv 2b_iT_0/eN_0$ is the ambipolar diffusion coefficient. The function $\tilde{z}$ models the three dominant ionization/recombination mechanisms: electron-impact ionization, three-body recombination, and wall recombination (radial diffusion). The equilibrium condition is $\tilde{z} = 0$ [Eq. (8)]. Linearizing Eq. (19) yields

$$\frac{\partial n_2^e}{\partial t} + \mathbf{V}_{0z}^e\cdot\nabla n_2^e + N_0\nabla\cdot\mathbf{v}_2^e = \left(\frac{\partial z}{\partial N_0}n_2^e + \frac{\partial z}{\partial T_0}T_2^e + \frac{\partial z}{\partial N_a}n_2^a\right)N_0 \equiv \tilde{z}_2N_0, \tag{21}$$

where we have dropped terms involving gradients of equilibrium quantities, such as $\mathbf{v}_2^e \cdot \nabla N_0$, since they are small by $1/k_{mn}a \ll 1$ compared to the retained terms.

The relative effect of the neutral particle fluctuations may be seen by summing all of the momentum equations:

$$0 = \nabla(P_e + P_i + P_a). \tag{22}$$

Since the total pressure is constant and $N_a/N_0 \gg 1$, the plasma pressure $P_e + P_i$ rests against the neutrals. The linearized form of Eq. (22) is

$$0 = 2n_2^e T_0 + N_0(T_2^e + T_2^i) + N_a T_2^a + n_2^a T_0. \tag{23}$$

One expects $n_2^e/N_0 \gg T_2^e/T_0$ due to ionization nonlinearities and $T_2^e \gtrsim T_2^i \gtrsim T_2^a$. Equation (23) indicates that $(N_0/N_a)(n_2^e/N_0) \simeq -n_2^a/N_a$ which implies

$$\frac{n_2^a}{N_a} \ll \frac{n_2^e}{N_0}.$$

Consequently, the fluctuations in the neutral density in Eq. (21) may be neglected by virtue of $N_0/N_a \ll 1$.

In the limit of an approximate Saha balance, $SN_a \simeq \beta N_0^2$ and $\tilde{z}_2$ has the form

$$\tilde{z}_2 = \frac{T_2^e}{T_0} z_t + n_2^e z_e + n_2^a z_a, \tag{24}$$

$$z_t \equiv \frac{ST_0 N_a^2}{N_0} \frac{\partial}{\partial T_0}[F(T_0)], \tag{25}$$

$$-\frac{z_e}{2} = z_a \frac{N_a}{N_0} = S_0 N_a, \tag{26}$$

where $(N_0)^2/N_a = S_0/\beta_0 = F(T_0)$ is the Saha equation[21, 39] and SN_a is the electron impact ionization rate given by[33]

$$S(T_e)N_a = N_a \frac{10^{-5}(T_e/I_0)^{1/2}}{I_0^{3/2}(6 + T_e/I_0)} \exp(-I_0/T_e) \quad \sec^{-1} \tag{27}$$

where I_0 and T_e are in units of eV and N_a is in units of cm^{-3}. In the opposite limit where wall recombination dominates three-body recombination ($SN_a = D_a/a^2$), the RHS of Eq. (24) has the form

$$z_t = N_a \frac{\partial S}{\partial T}, \tag{28}$$

$$z_e = -\frac{1}{a^2} \frac{\partial D_a}{\partial N_e}, \tag{29}$$

$$z_a = S - \frac{1}{a^2} \frac{\partial D_a}{\partial N_a}. \tag{30}$$

Linearization of the momentum Eqs. (6) and (7) yield

$$\mathbf{v}_2^e = -b_e \left(\mathbf{E}_2 + \frac{T_0 \nabla n_2^e}{eN_0} + \frac{\nabla T_2^e}{e} \right) - \mathbf{E}_0 \frac{\partial b_e}{\partial N_0} n_2^e, \tag{31}$$

$$\mathbf{v}_2^i = b_i \left[\mathbf{E}_2 - \frac{e(\nu_{ei} + \nu_{ea})}{T_0 \nu_{ea}} \left(\frac{\nabla n_2^e}{N_0} + \frac{\nabla T_2^i}{T_0} \right) - \frac{e\nu_{ei}}{T_0 \nu_{ea}} \left(\frac{\nabla n_2^e}{N_0} + \frac{\nabla T_2^e}{T_0} \right) \right] + \mathbf{E}_0 \frac{\partial b_i}{\partial N_0} n_2^e, \tag{32}$$

where we have ignored $\partial b_j/\partial T_0$ terms since $n_2^e/N_0 \gg T_2^e/T_0$. The ambipolar electric field $\mathbf{E}_2$ (recall that the beat wave is assumed to be quasineutral) arises due to the different mobilities of the electrons and ions. In order to maintain a divergence free current density, $\nabla \cdot \mathbf{J} = 0$, an ambipolar field is generated which drags the ions with the electrons. The ambipolar electric field is calculated from the constraint

$$\nabla \cdot \mathbf{J}_2 = 0 = eN_0 \nabla \cdot (\mathbf{v}_2^i - \mathbf{v}_2^e) + e(\mathbf{v}_0^i - \mathbf{v}_0^e) \cdot \nabla n_2^e, \tag{33}$$

where the gradients of equilibrium quantities have been ignored by virtue of $1/k_{mn}a \ll 1$. For finite beat-wave wave numbers $k_{mn} \neq 0$, Eq. (33) may be written as

$$0 = eN_0(\mathbf{v}_2^i - \mathbf{v}_2^e) + en_2^e(\mathbf{v}_0^i - \mathbf{v}_0^e). \tag{34}$$

Substituting $\mathbf{v}_0^e = -b_e \mathbf{E}_0$ and $\mathbf{v}_0^i = b_i \mathbf{E}_0$, the ambipolar field may be calculated using Eqs. (34), (32), and (31) to be

$$\begin{aligned} -\mathbf{E}_2(b_e + b_i) = &\left[(b_i + b_e)\mathbf{E}_0 + \mathbf{E}_0 \frac{\partial}{\partial N_0}(b_e + b_i) - b_i \frac{T_0}{e} \left(\frac{2\nu_{ei} + \nu_{ea}}{\nu_{ea}} \right) \nabla + \frac{b_e T_0}{e} \nabla \right] \frac{n_2^e}{N_0} \\ &- b_i \frac{T_0(\nu_{ei} + \nu_{ea})}{e\nu_{ea}} \nabla \frac{T_2^i}{T_0} + \frac{T_0}{e} \left(b_e - b_i \frac{\nu_{ei}}{\nu_{ea}} \right) \nabla \frac{T_2^e}{T_0}. \end{aligned} \tag{35}$$

Substituting Eq. (35) into Eq. (31), the velocity perturbation becomes

$$\mathbf{v}_2^e = \left[b_e E_0 - \frac{b_i T_0}{e} \left(1 + \frac{2\nu_{ei} + \nu_{ea}}{\nu_{ea}} \right) \nabla \right] \frac{n_2^e}{N_0} - \frac{b_i T_0}{e} \left(1 + \frac{\nu_{ei}}{\nu_{ea}} \right) \nabla \frac{T_2^e}{T_0} - \frac{b_i T_0}{e} \nabla \frac{T_2^i}{T_0}, \tag{36}$$

where $b_e \gg b_i$ has been used.

Combining the continuity Eq. (21) and (36) and noting that neutral fluctuations are small by $N_0/N_a \ll 1$, yields the diffusionlike equation for continuity

$$\frac{\partial n_2^e}{\partial t} - D_i(1+c_1)\nabla^2\frac{n_2^e}{N_0} - D_i(1+c_2)\nabla^2\frac{T_2^e}{T_0} = z_t T_2^e + z_e n_2^e, \tag{37}$$

where $D_i \equiv b_i T_0/eN_0 \simeq D_a/2$ is the ion-diffusion coefficient (half of the ambipolar diffusion coefficient), $c_1 = (2\nu_{ei}+\nu_{ea})/\nu_{ea}$, and $c_2 = [H_i(\nu_{ei}+\nu_{ea})+\nu_{ei}]/\nu_{ea}$ [H_i to be defined by Eq. (41)]. As is expected, in the absence of any ionization source in Eq. (37), density fluctuations decay on the time scale of the ambipolar diffusion rate.

Fourier analyzing Eq. (37) yields the plasma density fluctuations due to temperature fluctuations (with $\partial/\partial t \to 0$ for DFWM limit)

$$\frac{n_2^e}{N_0} = \frac{T_2^e}{T_0}\frac{[T_0 z_t - D_i k_{mn}^2(1+c_2)]}{[-N_0 z_n + D_i k_{mn}^2(1+c_1)]}. \tag{38}$$

In the limit that the ambipolar diffusion rate is much larger than the ionization rates $k_{mn}^2 D_i \gg T_0 Z_t, N_0 z_n$, Eq. (38) reduces to the thermal force limit $N_2^e/N_0 = -T_2^e/T_0$. In order to achieve significant ionization beat wave, we require

$$k_{mn}^2 D_i \ll T_0 z_t \simeq \frac{I_0}{T_0} S N_a.$$

Also note from Eq. (38) that while the peaks of maximum density and temperature fluctuations are out of phase in the thermal force limit, the peaks coincide in the ionization force limit.

One may identify three different ionization balance regimes of Eq. (38) depending on the equilibrium ionization balance and the rate of plasma production by electron-impact ionization. As just mentioned, when the diffusion rate through a beat-wave is fast compared to the ionization rate, Eq. (38) reduces to the thermal force limit. In the limit of approximate Saha balance, $N_0 N_a S \simeq N_0^3 \beta$ and $T_0 z_t \simeq S N_a I_0/T_0$ and $N_0 z_n \simeq S N_a$ so that Eq. (38) has the form

$$\frac{n_2^e}{N_0} = \frac{T_2^e}{T_0}\frac{[S N_a I_0/T_0 - D_i k_{mn}^2(1+c_2)]}{[2S N_a + D_i k_{mn}^2(1+c_1)]}.$$

If the rate of ambipolar diffusion is much smaller than the ionization rate ($D_i k_{mn}^2 \ll S N_a$), then the beat wave is dominated by the ionization nonlinearity and $n_2^e/N_0 \simeq (T_2^e/T_0)(I_0/T_0)$. The relation

$$D_i k_{mn}^2 \ll S N_a \tag{39}$$

determines the minimum beat-wave wavelength which sustains an approximate Saha balance for the beat wave. In terms of a single-particle picture, Eq. (39) requires the ionization rate to be large compared to the rate at which neutral species diffuse through a beat-wave wavelength. In this regime, the neutral species diffuse slowly enough to sample the impressed temperature perturbation.

When the electron-impact ionization is balanced by wall recombination, Eq. (38) has the form

$$\frac{n_2^e}{N_0} \simeq \frac{T_2^e}{T_0}\frac{[(I_0/T_0)D_a/a^2 - D_a k_{mn}^2]}{(D_a/a^2 + D_a k_{mn}^2)}$$

$$\simeq \frac{T_2}{T_0}\left(\frac{I_0}{T_0}\frac{1}{k_{mn}^2 a^2} - 1\right) \sim -\frac{T_2^e}{T_0}$$

with $1/k_{mn}^2 a^2 \ll 1$. *Clearly when wall recombination becomes important, the strength of the ionization nonlinearity is greatly reduced.* Consequently, all of the examples presented in Sec. IV will focus on the Saha ionization balance limit.

In this paper, only the DFWM $\partial/\partial t \to 0$ beat-wave response is considered. For a completely ionized plasma, the sound wave frequency is the typical DFWM response time [4, 3, 1]. However, when ionization nonlinearities dominate, the DFWM response time of the beat-wave response is determined by the electron-impact ionization rate SN_a as shown by inspection of the plasma continuity

$$N_0 \tilde{z}_2 = \frac{\partial n_2^e}{\partial t} + N_0 \nabla \cdot \mathbf{v}_2^e + \mathbf{V}_{0e} \cdot \nabla n_2^e$$

and

$$\tilde{z}_2 = \frac{T_2^e}{T_0} S N_a - 2 n_2^e S_0 N_a + n_2^a S_0 N_0,$$

where $N_0 \nabla \cdot \mathbf{v}_2^e + \mathbf{V}_{0e} \cdot \nabla n_2^e$ scales as the ambipolar diffusion rate. Physically, this means that the ionization nonlinearity can only respond as fast as the ionization rate. Approximate response times are listed for the given examples.

As with the continuity equation, the perturbation to the radial loss terms may be neglected in the beat-wave energy equations since they are smaller than the retained terms by factors of $1/k_{mn}a \ll 1$. The energy equations may be further simplified by noting that the temperature fluctuations T_2^a and T_2^i are no larger than T_2^e. Therefore, we define the parameters

$$T_2^a = H_a T_2^e, \tag{40}$$

$$T_2^i = H_i T_2^e \tag{41}$$

with H_a, H_i constant and $0 \le H_a, H_i \simeq 1$. For the purposes of this paper, the exact values of H_a and H_i are unimportant. In the limit that the energy transfer to the ions and neutral species is small compared to the rate at which the electrons themselves transport the heat, then $H_a = H_i = 0$. In the other limit that the energy is efficiently transferred to the other species, $H_i \simeq H_a \simeq 1$. Summing the energy equations yields

$$0 = Q_{\mathrm{BW}} + \kappa^t \nabla^2 T_2^e + \mathbf{J}_0 \cdot \mathbf{E}_2 - N_0 \tilde{z}_2 I_0 - T_0 N_0^e \nabla \cdot \mathbf{v}_2^e \tag{42}$$

where $\kappa^t = \kappa^e + H_i \kappa^i + H_a \kappa^a$ is the total thermal conduction of the plasma and Q_{BW} represents the beat-wave heating term. The beat-wave heating term,

$$Q_{\mathrm{BW}} = 0.51 m_e N_0(\nu_{ei}+\nu_{ea})\exp(i\mathbf{k}_{mn}\cdot\mathbf{r} - i\omega_{mn}t)\sum_{m,n}\mathbf{v}^e_{1m}\cdot\mathbf{v}^{e*}_{1n} + \text{c.c.}, \tag{43}$$

includes electron-atom collisions. The sum in the beat-wave heating term follows the notation of Refs. [3, 4]. The first two terms on the right-hand side (RHS) in the electron energy Eq. (42) combine to yield the familiar thermal force for DFWM in plasmas. The $N_0\tilde{z}_2$ terms in the energy equations account for the loss or gain of energy in plasma production. To a good approximation, radiation losses may be neglected in the energy equations [4].

The resultant DFWM beat-wave response from Eqs. (38), (42), (35), and (36) is

$$\frac{n^e_2}{N_0} = \frac{\tilde{Q}_{\mathrm{BW}}}{N_0T_0}\frac{\Psi}{\Phi}, \tag{44}$$

$$\Psi \equiv \frac{[T_0z_t - D_ik^2_{mn}(1+c_2)]}{[-N_0z_n + D_ik^2_{mn}(1+c_1)]}, \tag{45}$$

$$\Phi \equiv \frac{k^2_{mn}\kappa^t}{N_0} + \frac{I_0T_0z_t}{T_0} + \frac{ik_{mn}J_0}{eN_0} + \Psi\left[n_0z_n\frac{I_0}{T_0} + \frac{J_0E_0}{N_0T_0}\left(1+\frac{N_0}{b_e}\frac{\partial b_e + b_i}{\partial N_0}\right) - 2\frac{ikJ_0}{eN_0} - k^2_{mn}D_i(1+c_1)\right], \tag{46}$$

where $\tilde{Q}_{\mathrm{BW}}$ is the fourier component $0.51m_eN_0(\nu_{ei}+\nu_{ea})\sum_{m,n}\mathbf{v}^e_{1m}\cdot\mathbf{v}^{e*}_{1n}$ and $B_n \equiv N_0\partial b_e/\partial N_0 b_e$. This expression may be simplified by noting that J_0E_0/N_0T_0 scales as κ^e/N_0a^2 from the equilibrium Eq. (10). Consequently, this term may be neglected by virtue of $1/k_{mn}a \ll 1$. In addition, we neglect the $ik_{mn}J_0/eN_0$ terms compared to the $k^2_{mn}\kappa^t/N_0$ term. Noting that $J_0/eN_0 \simeq b_eE_0 = eD_eE_0/T_0$ and the thermal conductivity term may be approximated by the electron diffusion to the wall $\kappa^t \simeq \kappa^e \simeq D_e/N_0$, neglecting the $ik_{mn}J_0/eN_0$ term is equivalent to

$$\frac{eE_0}{k_{mn}T_0} \ll 1.$$

This inequality is typically true for electric gas discharges. For typical values of [40, 19] $E_0 \sim 10$ V/cm, $a \sim 1$ cm, $T_0 \sim 2$ eV, we estimate $(eE_0a/T_0)(1/k_{mn}a) \simeq 5/k_{mn}a \ll 1$.

In addition, the other terms in Φ are also usually small compared to the thermal conduction term, so that the beat-wave response has the form

$$\frac{n^e_2}{N_0} = \frac{\tilde{Q}_{\mathrm{BW}}}{N_0T_0}\frac{N_0}{k^2_{mn}\kappa^t}\frac{[T_0z_t - D_ik^2_{mn}(1+c_2)]}{[-N_0z_n + D_ik^2_{mn}(1+c_2)]}, \tag{47}$$

$$\simeq \frac{\tilde{Q}_{\mathrm{BW}}}{N_0T_0}\frac{N_0}{k^2_{mn}\kappa^t}\frac{I_0}{T_0} \qquad (SN_a \gg D_ik^2_{mn}) \tag{48}$$

as was anticipated using the simple derivation in the Introduction.

IV. ESTIMATION OF PHASE CONJUGATE REFLECTIVITY

Using argon and cesium plasmas as examples, phase-conjugate reflectivities for the ionization nonlinearity are estimated. As is a usual practice for estimating nonlinearities, we choose laser intensities which result in reflectivities just below unity. The results in this section may be scaled to smaller pump powers by noting that the reflectivity scales as the square of the pump intensity.

Using the electron beat-wave response calculated in this paper, the reflectivity is estimated using [9, 10]

$$R = \frac{\kappa^2\tan^2(\kappa_eL)e^{-2\alpha L}}{|\alpha\tan(\kappa_eL) + |\kappa_e||^2}, \tag{49}$$

$$\kappa_e = (\kappa^2e^{-2\alpha L} - \alpha^2)^{1/2}, \tag{50}$$

$$\kappa = \left|\frac{2\pi\omega_b}{cn_o}\chi^{(3)}E_fE_b\right|, \tag{51}$$

as discussed in Refs. [4, 3], where n_0 is the linear index of refraction and L is the interaction length. The nonlinear susceptibility is calculated from $\partial\mathbf{P}_3/\partial t = \mathbf{J}_3 \simeq -en^e_2\mathbf{v}^e_1$ and Eq. (11). The various charged particle-neutral collision frequencies are estimated using the elastic scattering cross-section data listed in Table I. The collision frequencies are approximated as

$$\nu_{jl} = v_{tj}N_l\sigma_{jl},$$

where v_{tj} is the thermal velocity of the jth species (with the appropriate reduced mass), N_l is the density of the target species, and σ_{jl} is the cross section. The thermal conductivities are estimated from [41]

$$\kappa^e = 3.2\frac{N_0v^2_{te}}{\nu_{ei}+c_3\nu_{ea}},$$

$$\kappa^i = 3.9\frac{N_0v^2_{ti}}{\nu_{ii}+c_4\nu_{ia}},$$

$$\kappa^a = 3\frac{N_av^2_{ta}}{\nu_{ai}+\nu_{aa}}.$$

Using the general form for the electron density beat wave Eqs. (44)–(46) with $J_0 = 0$, and Eqs. (49)–(51), the expected reflectivity may be calculated for various plasma parameters. For the high gas pressure considered in the following examples, there is an approximate Saha ionization balance so that $SN_a \simeq \beta N_0^2$. For a given equilibrium temperature, there are a range of equilibrium electron densities which satisfy the approximate ionization balance. Consequently, for simplicity, the equilibrium temperature and neutral gas densities are held constant and the phase-conjugate reflectivity is plotted as a function of electron density.

TABLE I. Experimental elastic scattering cross sections.

10^{-16} cm^2	1 eV	4 eV	10^{-16} cm^2	0.3 eV	1 eV
$\sigma_{e\,Ar}$	2[a]	5.6	$\sigma_{e\,Cs}$	340[b]	280
$\sigma_{Ar+\,Ar}$	40	35	$\sigma_{Cs+\,Cs}$	4500[c]	3000
$\sigma_{Ar\,Ar}$	1[d]	1[d]	$\sigma_{Cs\,Cs}$	450[e]	300[e]

[a]Data for Argon cross sections from Ref. [45], pp. 27 and 41.
[b]Data for $\sigma_{e\,Cs}$ from Ref. [46], p. 6.
[c]Data for $\sigma_{Cs+\,Cs}$ from Ref. [39], p. 109 (includes charge exchange).
[d]Estimated (geometric).
[e]Estimated to be comparable to $\sigma_{e\,Cs}$.

Figure 3 shows the expected reflectivity using CO_2 lasers in a weakly ionized cesium plasma. The solid curve represents the expected reflectivity for a completely ionized plasma at the same electron density and temperature ($N_a = 0$). The lower dashed curve is calculated assuming that only the thermal conduction and collision frequencies of the plasma are modified by the neutral species (no ionization). The upper dashed curve represents the expected reflectivity due to the ionization nonlinearity in a weakly ionized plasma ($N_a = 5 \times 10^{17}$ cm^{-3}). The enhancement of the reflectivity from a weakly ionized plasma compared to a completely ionized plasma demonstrates that ionization nonlinearities are stronger than thermal pressure nonlinearities. The DFWM response time, as determined by the electron-impact ionization rate, is $1/SN_a \simeq 0.2$ nsec.

Other gases may be used for the plasma. Figure 4 illustrates expected reflectivities for a weakly ionized argon plasma. The equilibrium temperature for the argon plasma is 4 eV so that the ionization rate, which scales as $\exp(I_0/T_0)$, is approximately the same for the argon and cesium plasmas. (DFWM response time $1/SN_a \simeq 0.2$ nsec.)

Similar curves may be obtained for EM wavelengths of 119 μm (Fig. 5 DFWM response time $1/SN_a \simeq 5$ nsec). Note that the thermal force reflectivity scales as N_0^6 in the 10.6 μm and 119 μm figures, while the ionization force reflectivity scales as N_0^2. The N_0^2 scaling is a consequence of the electron-neutral collisions determining the electron mean free path. This scaling may be easily seen from the electron density beat-wave response

$$\frac{n_2^e}{N_0} = -\frac{v_{osc}^2}{v_{te}^2}\left(1 + \frac{N_0\nu_{ei}}{k_{mp}^2\kappa^e} - \frac{N_0(\nu_{ei}+\nu_{ea})}{k_{mp}^2\kappa^t}\frac{I_0}{T_0}\right).$$

The three terms in the large parentheses represent the ponderomotive, thermal, and ionization forces, respectively. When the neutral density is low, $\nu_{ea} \ll \nu_{ei}$, $\kappa^t \rightarrow \kappa^e$ and the ionization nonlinearity term reduces to

$$n_2^e \simeq N_0\frac{v_1^2}{v_{te}^2}\frac{N_0\nu_{ei}}{k_{mp}^2\kappa^e}\frac{I_0}{T_0} \simeq \frac{N_0^3\lambda^4 S N_a^2}{T_0^5}\left(\frac{I_0}{T_0}\right),$$

and the reflectivity scales as $(n_2^e)^2 \simeq N_0^6$. However, when

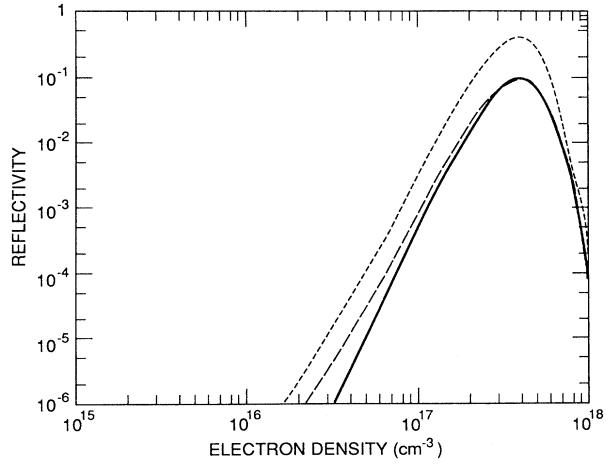

FIG. 3. Reflectivity for ionization nonlinearity in cesium plasma at 10.6 μm. Interaction length is 5 cm; $T_e = 1$ eV; $I = 400$ kW/cm^2; interaction angle is 5° (k_{fp} grating). The solid curve is the expected reflectivity for $N_a = 0$. The long-dashed curve represents the reflectivity assuming that the only effect of the neutral species is to modify the collision frequencies (no ionization). The upper short-dashed curve represents the expected reflectivity for ionization nonlinearity ($N_a = 5 \times 10^{17}$ cm^{-3}).

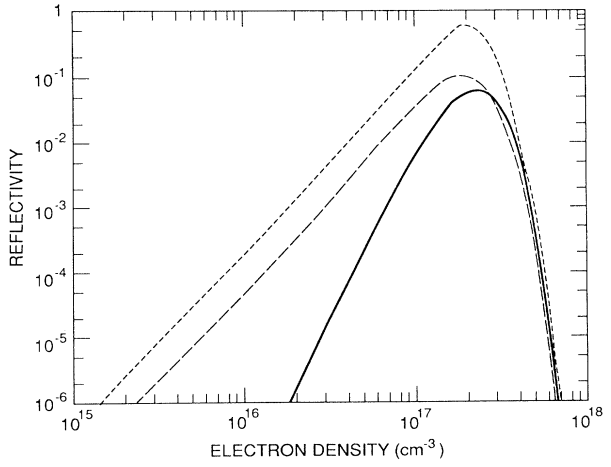

FIG. 4. Reflectivity for ionization nonlinearity in argon plasma at 10.6 μm. Interaction length is 5 cm; $T_e = 4$ eV; $I = 6$ MW/cm^2; interaction angle is 2° (k_{fp} grating); $N_a = 10^{18}$ cm^{-3}. Same notation for the different curves as in Fig. 3.

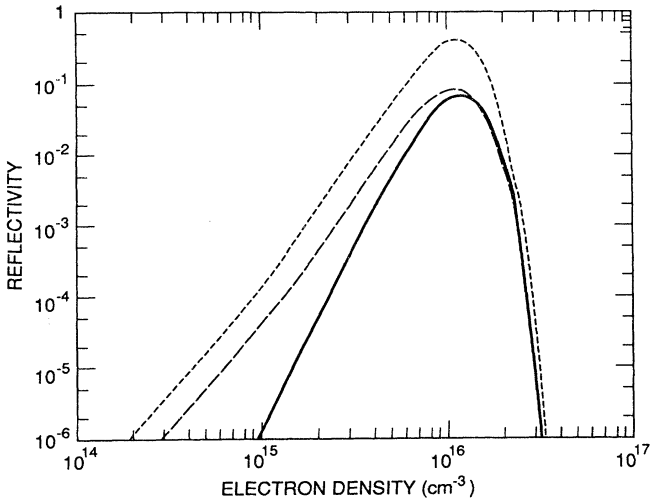

FIG. 5. Reflectivity for ionization nonlinearity in cesium plasma at 119 μm. Interaction length is 5 cm; $T_e = 1$ eV; $I = 60$ kW/cm^2, interaction angle is 15° (k_{fp} grating); $N_a = 2 \times 10^{16}$ cm^{-3}. Same notation for the different curves as in Fig. 3.

$\nu_{ea} \gg \nu_{ei}$, the electron mean free path is determined by the electron-neutral collisions and the nonlinearity scales as approximately

$$n_2^e \simeq N_0 \frac{v_1^2}{v_{te}^2} \frac{\nu_{ea}^2}{k_{mp}^2 v_{te}^2} \frac{I_0}{T_0} \simeq \frac{N_0 \lambda^4}{T_0} \left(\frac{I_0}{T_0}\right).$$

Since the neutral species, rather than a large ion density, maintain the plasma in a collisional regime, the reflectivity scales like $(n_2^e)^2 \simeq N_0^2$. *Consequently, ionization nonlinearities may dominate ponderomotive nonlinearities for low electron densities* (corresponding to long EM wavelengths). Moreover, small interaction angles are not

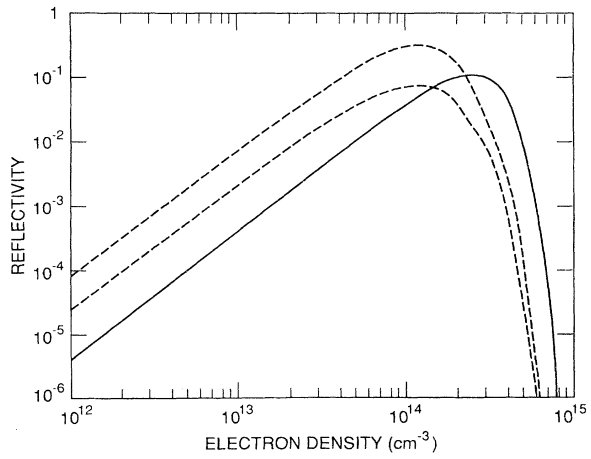

FIG. 6. Reflectivity for ionization nonlinearity in cesium plasma at 1 mm. Interaction length is 50 cm; $T_e = 1$ eV; $I = 64$ kW/cm^2; interaction angle is 0° (k_{bp} grating only); $N_a = 10^{16}$ cm^{-3}. Same notation for the different curves as in Fig. 3.

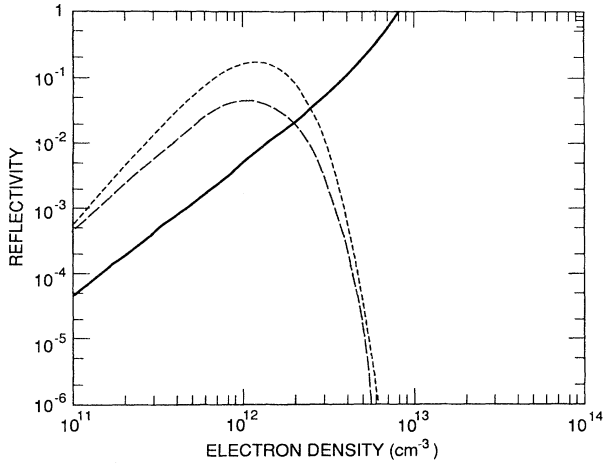

FIG. 7. Reflectivity for ionization nonlinearity in cesium plasma at 1 cm. Interaction length is 100 cm; $T_e = 1$ eV; $I = 1$ kW/cm^2; interaction angle is 0 ° (k_{bp} grating only); $N_a = 10^{16}$ cm^{-3}). Same notation for the different curves as in Fig. 3.

required for one of the beat waves to be in a collisional regime; even the small scale grating can be in the collisional regime due to electron-neutral collisions.

Estimated reflectivities for 1 mm and 1 cm waves are illustrated in Figs. 6 and 7 ($1/SN_a \simeq 10$ nsec). The solid curves in these figures (no neutral species) scale as N_0^2 since the 100% ionized plasma is dominated by ponderomotive nonlinearities for collinear interaction ($\theta = 0$ k_{bp} grating only). As with Figs. 6 and 7, the electron-neutral collisions determine the electron mean free path.

V. STABILITY OF EQUILIBRIUM

As discussed in Refs. [4, 19, 18, 28], weakly ionized gas-discharge plasmas naturally tend to break into striations due to an ionization instability. Likewise, laser driven optical striations are also unstable as described in Refs. [30–32] due to a similar ionization instability. Therefore, in order to ascertain the suitability of weakly ionization plasmas for four-wave mixing and phase conjugation, a stability analysis of the equilibrium plasma is necessary.

The purpose of this section is to examine the tendency of the plasma to break into striations in the axial direction and to estimate the joule and laser heating power thresholds for the instability. A threshold laser heating rate implies a maximum permissible pump power before the equilibrium plasma becomes unstable. Does this maximum pump power limit the attainable phase-conjugate reflectivity using ionization nonlinearities?

References [18, 31, 28] provide a detailed discussion of the plasma stability for electric discharge plasmas. We use the same equations as Ref. [18] to illustrate the effect of the stability on the FWM process by estimating the threshold laser intensity for the onset of striation and the corresponding maximum phase-conjugate reflectivity at that threshold intensity. The equations used in this paper

are somewhat simplified from those of Ref. [18] since the role of metastable atoms (stepwise ionization) is ignored in this paper. Since metastables play a major role in the stability of gas discharges, the model stability equations shown below are inherently stable in the absence of the laser heating. Neglecting the role of metastables is not a very restrictive condition, however, since there are some gases, such as alkali plasmas (recall that most of the examples in Sec. IV were cesium plasmas), which do not have metastable states [18].

The model equations are

$$\frac{\partial n_e}{\partial t} + \nabla(n_e \mathbf{V}_e) = n_e \tilde{z}, \tag{52}$$

$$\frac{\partial}{\partial t}(\tfrac{3}{2} n_e T_e) + \nabla(\tfrac{3}{2} T_e N_e \mathbf{V}_e^*) = -\mathbf{J}\cdot\mathbf{E} + Q_{\text{laser}} - n_e H, \tag{53}$$

$$\mathbf{V}_p = b_i \mathbf{E}, \tag{54}$$

$$\mathbf{V}_e = -b_e \left(\mathbf{E} + T_e \frac{\nabla n_e}{n_e} + (\eta - \tfrac{3}{2}) \nabla T_e \right), \tag{55}$$

$$\mathbf{V}_e^* = -\tfrac{2}{3}\eta b_e \left(\mathbf{E} + T_e \frac{\nabla n_e}{n_e} + (\eta^* - \tfrac{3}{2}) \nabla T_e \right), \tag{56}$$

$$\nabla \cdot \mathbf{J} = \nabla[e N_e (\mathbf{V}_p - \mathbf{V}_e)] = 0, \tag{57}$$

where η and η^* are determined by the dependence of the electron mean free path on the velocity and the form of the velocity distribution function. For a Maxwellian distribution, $\eta = 2$ and $\eta^* = 3$ [42]. The Q_{laser} term in the energy equation represents the laser heating of the plasma. As discussed in Sec. III, we have included the radial losses in the continuity and energy equations in the form of a model radial loss term. The RHS of Eq. (52) follows the same notation as Eq. (21). The radial energy-loss term $n_e H$ scales as the electron thermal conduction time to the walls ($N_e H \simeq \kappa^e T_0/a^2 \simeq N_0 T_0 D_e/a^2$).

The geometry of the cylindrically symmetric equilibrium plasma is depicted in Fig. 8. The plasma is assumed

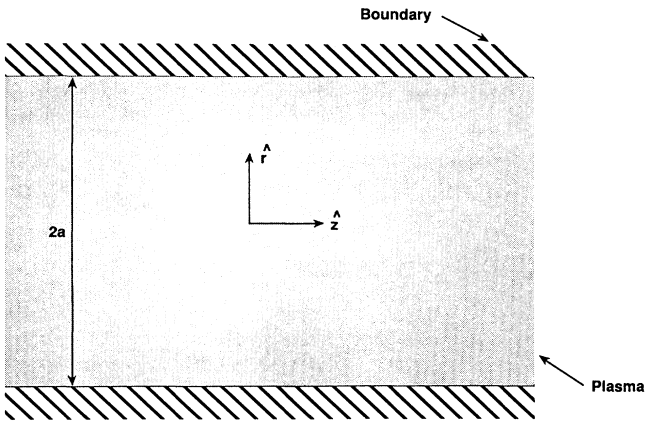

FIG. 8. Geometry for stability analysis of weakly ionized plasma.

to be initially uniform in the parallel direction. Since all of the radial motion has been included in the $\tilde{z}$ and $n_e H$ terms, the gradients and time derivative refer to the formation of striations in the axial direction. The parallel equilibrium solution ($\partial/\partial t = 0$) of Eqs. (52)–(57) is the same as described in Sec. II:

$$\tilde{z} = 0, \tag{58}$$

$$\mathbf{v}_{e0} = -b_e \mathbf{E}_0, \tag{59}$$

$$\mathbf{v}_{i0} = b_i \mathbf{E}_0, \tag{60}$$

$$\mathbf{J} = e N_0 (b_e + b_i) \mathbf{E}_0. \tag{61}$$

The equilibrium energy balance may be approximated as

$$J_0 E_0 + Q_0 = N_0 H. \tag{62}$$

Following the analysis of Sec.III and Ref. [18], the perturbed Eqs. (52)–(57) may be Fourier transformed in the parallel direction and in time [$\exp(i\omega t - ikz)$]. The resulting density and temperature perturbations equations, which include laser heating are a generalization of Nedospasov's equations [18]. Combining the perturbation equations with $\omega \simeq D_a k^2 \ll k J_0/e N_0$ and equating real and imaginary parts yields [4] the real and imaginary frequencies $\omega = \omega_r - i\gamma$.

$$\omega_r \simeq \frac{k b_e E_0 T_0 z_t}{\partial H/\partial T_0 + \eta(\eta^* - \eta) D_e k^2} \simeq k b_i E_0 \qquad (\text{for} \quad ka \sim 1), \tag{63}$$

$$\gamma \simeq -D_a k^2 + N_0 z_n - z_t T_0 \frac{J_0 E_0 [2 + N_0 \partial(b_e + b_i)/b_e \partial N_0]/N_0 T_0 + Q_0(1 - Q_n)/N_0 T_0}{\partial H/\partial T_0 + \eta(\eta^* - \eta) D_e k^2}, \tag{64}$$

where $\gamma > 0$ corresponds to instability and

$$Q_n \equiv \frac{N_0}{Q_0}\frac{\partial Q_0}{\partial N_0} > 0, \tag{65}$$

$$Q_t \equiv \frac{T_0}{Q_0}\frac{\partial Q_0}{\partial T_0} < 0, \tag{66}$$

where Q_n and Q_t are numbers of order unity and $Q_0 \simeq m_e N_0 (\nu_{ei} + \nu_{ea}) v_{\text{osc}}^2$. In the analysis, the equilibrium condition $J_0 E_0 + Q_0 = N_0 H$ and $b_e \gg b_i$ has been used. The frequency of the striation, Eq. (63) is not affected by the laser heating (as expected since optical striations are inherently stationary) and therefore reduces to the same

expression as in Ref. [18]. In the limit of no laser heating ($Q_0 = 0$) and $z_n = 0$ (wall recombination dominates three-body recombination), the damping rate Eq. (64) reduces to the Nedospasov result for damped striations (metastables neglected).

Returning to Eq. (64) for the growth rate, let us examine the $J_0 = 0$ limit of optical striations. In this limit, the $k = 0$ modes are unstable if $Q_n > 1$ and

$$\frac{\partial H}{\partial T_0}\frac{|z_n N_0|}{T_0 z_t} \simeq \frac{H I_0}{T_0^2} < \frac{Q_0}{N_0 T_0}|1 - Q_n|.$$

Therefore, in the absence of the Joule heating, the plasma is more susceptible to striations. We further note that if the $N_e H$ term in the energy Eq. (53) were independent of electron density and $z_n = 0$, as assumed in Ref. [30], the plasma would always be unstable, independent of equilibrium conditions. This instability behavior in the $J_0 = 0$, and $k = 0$ limit confirms a similar analysis of optical striations by Nastoyashchii [30].

By examination of Eq. (64) we require

$$\frac{J_0 E_0}{N_0 T_0} \simeq \frac{H}{T_0} > \frac{Q_0}{N_0 T_0}$$

for stability of the equilibrium plasma for all wavelengths in the presence of laser heating. The threshold laser power is then

$$\left.\frac{Q_0}{N_0 T_0}\right|_{\text{thres}} = \frac{H}{T_0} \sim \frac{\kappa^e}{N_0 a^2}. \tag{67}$$

The equilibrium laser heating rate $Q_0/N_0 T_0$ must be small compared to the thermal diffusion rate to the wall in order for the plasma equilibrium to be stable. As long as the EM waves do not disturb the equilibrium, the plasma should be suitable for wave mixing. Substituting Eq. (67) into the expression for the beat-wave amplitude Eq. (48), and using the small signal reflectivity limit

$$R \simeq \left(\frac{n_2^e L N_0}{N_0 \lambda N_c}\right)^2$$

the maximum reflectivity is estimated to be

$$R_{\max} = \left(\frac{I_0}{T_0}\right)^2 \frac{I_p}{I_f}\frac{1}{k_{mn}^2 a^2}\left(\frac{L\lambda_{mn}}{a\lambda}\right)^2 \frac{N_0^2}{N_c^2} \tag{68}$$

where L is the interaction length, λ is the EM wavelength, N_c is the critical density, and $1/k_{mn}^2 a^2 \ll 1$. In order to maximize the reflectivity, one requires a plasma with $I_0/T_0 \gg 1$, electron densities close to the critical density, beat-wave wavelengths long compared to the EM wavelength, and long interaction lengths compared to the radial extent of the plasma (e.g., a long cylindrical plasma with $L \gg a$). The maximum reflectivity tends to decrease with increasing radial extent of the plasma since the thermal relaxation rate H/T_0 becomes much longer in large radius plasmas resulting in a lower intensity threshold for the onset of striations.

Does the laser intensity threshold for the onset of striations limit the attainable phase-conjugate reflectivities in the gas-discharge plasmas cited in Sec. IV? As an example, consider the plasma parameters of Fig. 6 with $N_0 = 10^{14}$ cm^{-3}, $T_e = 1$ eV, $I = 64$ kW/cm^2 for 1 mm waves. We estimate the heating of the pump beams as $Q_0 \simeq 0.5 m_e(\nu_{ei} + \nu_{ea}) N_0 v_{\text{osc}}^2 \simeq 4 \times 10^{10}$ erg/sec cm^3. From the stability analysis in this section, we estimate the required equilibrium electric field as $J_0 E_0 = e b_e N_0 E_0^2 \simeq Q_0$. For the parameters of Fig. 6, $E_0 \simeq 38$ V/cm which is about an order of magnitude above typical gas-discharge electric fields of 1–10 V/cm. The radius of the discharge is estimated from $J_0 E_0 \simeq \kappa^e T_e / a^2 \simeq 3.2 D_e N_0 T_0 / a^2$ to be $a \simeq 0.025$ cm which is a factor of 10 smaller than typical values of 1–10 mm. Since the heating by the pump beams implies equilibrium electric fields which are about an order of magnitude too large and plasma radiuses which are too small, we may surmise that reflectivities close to unity as in Fig. 6 are not possible for typical gas-discharge parameters.

What are typical expected reflectivities for gas discharge plasmas? For typical values of $a \simeq 0.25$ cm and $E_0 \simeq 4$ V/cm, we estimate $Q_0 \simeq 2.1 \times 10^8$ erg/sec cm^3 and $I_0 \simeq 340$ W/cm^2. Compared to Fig. 6, this intensity implies an expected reflectivity of 5×10^{-3}. Although the reflectivity is not very large, this reflectivity level should be experimentally observable. For example, phase conjugate reflectivities of $10^{-4} - 10^{-2}$ have been observed in plasmas (Ref. [6]).

Although large reflectivities are not expected in steady-state gas discharges, large reflectivities might be possible using *pulsed* plasma sources (as with Ref. [6]). With pulsed plasma sources, the issue of laser heating perturbing the plasma equilibrium and driving striations may not be a concern since striations are typically low frequency (10 kHz to dc) instabilities. A detailed analysis of a pulsed plasma source is beyond the scope of this paper.

As a final comment, even if the heating of the plasma by the pump beams does not excite striations, the equilibrium temperatures and densities could still be modified by the heating. Four-wave mixing is still possible under these conditions. However, the reflectivity will no longer scale as I^2 since the equilibrium temperature and density are functions of the pump beam intensity. An example of this effect for semiconductors is discussed in Ref. [26]. Below a threshold pump intensity, where the beat wave is generated by ionization forces, the reflectivity scales as I^2. Above the threshold intensity, the bulk (equilibrium) density of electron-hole pairs is significantly changed. In this regime, the reflectivity scales as I^{11}. A similar effect has also been observed in plasmas. In experiments with DFWM in collisional plasmas [6], the reflectivity does not scale as I^2 due to a suspected heating of the plasma by the pump beams.

VI. CONCLUSION

In summary, this paper has identified and studied the ionization nonlinearity as a new nonlinearity for DFWM in weakly ionized plasmas. (Although we have focused exclusively on DFWM, ionization nonlinearities may also play a role in other third order nonlinearities such as self-focusing.) Degenerate four-wave mixing using ionization nonlinearities may yield significant phase conjugate re-

flectivities depending on plasma conditions. In this paper, we focused on plasma parameters which are typical for steady-state gas-discharge plasmas.

More specifically, our results show that plasmas which are close to Saha ionization balance ($N_a S \simeq N_0^3 \beta$) have a stronger nonlinearity than plasmas in which the ionization balance is determined by diffusion or wall recombination. For equilibrium plasmas which are close to Saha equilibrium, the ionization nonlinearity may be stronger than either the thermal or ponderomotive nonlinearities due to strong electron-neutral collisions. Estimates of the phase-conjugate reflectivity indicate that gains $\lesssim 1$ are possible in weakly ionized plasmas. However, the stability condition of the equilibrium plasma may impose a laser intensity threshold for instability and thus limit the attainable phase conjugate reflectivities to $\sim 10^{-4}$ in steady-state plasma discharges. Higher reflectivities may be possible with pulsed plasma sources.

Plasma parameter regimes other than the steady-state gas discharge should exhibit analogous ionization nonlinearities. For example, multiphoton ionization processes might become important for sufficiently strong EM field intensities. In this regime, the ionization nonlinearity may be similar to the ionization nonlinearities in semiconductors [26]. As another example, there has been recent interest in the prospect of FWM and phase conjugation in the ionospheric plasma [43, 8]. In the upper ionosphere (D and E regions) where the weakly ionized plasma is collision dominated, photoionization as well as other ionization or recombination mechanisms may play a role in an analogous ionization nonlinearity.

ACKNOWLEDGMENTS

The authors acknowledge enlightening discussions with N. Fisch, C. Oberman, D. Mansfield, M. Goldman, and C. Joshi. This research was sponsored, in part, by the Strategic Defense Initiative, Office of Innovative Science and Technology and managed by Harry Diamond Laboratories. The authors also acknowledge the support of the Princeton Plasma Physics Laboratory under Department of Energy Contract No. DE-AC02-76-CHO-3073.

* Present address: AT&T Bell Laboratories, Room 6D225, 600 Mountain Ave., Murray Hill, NJ 07974.

[1] D. Steel and J. Lam, Opt. Lett. **4**, 363 (1979).
[2] Q. Zhong, Chin. Phys. **2**, 141 (1982).
[3] J. F. Federici and D. K. Mansfield, J. Opt. Soc. Am. B **3**, 1588 (1986).
[4] J. F. Federici, Ph.D. thesis, Princeton University, 1989.
[5] I. Nebenzahl, A. Ron, D. Tzach, and N. Rostoker, Phys. Fluids **31**, 2144 (1988).
[6] Y. Kitagawa, J. R. L. Savage, and C. Joshi, Phys. Rev. Lett. **62**, 151 (1989).
[7] T. Lehner, Phys. Scr. **39**, 595 (1989).
[8] M. V. Goldman and E. A. Williams, Phys. Fluids **3**, 751 (1991).
[9] R. A. Fisher, *Optical Phase Conjugation* (Academic, New York, 1985).
[10] B. Y. Zel'dovich, N. F. Pilipetsky, and V. V. Shkunov, *Principles of Phase Conjugation* (Springer-Verlag, New York, 1985).
[11] D. Rogovin and S. O. Sari, Phys. Rev. A **31**, 2375 (1985).
[12] R. McGraw and D. Rogovin, Phys. Rev. A **34**, 689 (1986).
[13] B. Bobbs, R. Shih, H. R. Fetterman, and W. W. Ho, Appl. Phys. Lett. **52**, 4 (1988).
[14] R. Shih, H. R. Fetterman, W. W. Ho, R. L. McGraw, D. N. Rogovin, and B. L. Bobbs, Proc. Soc. Photo-Opt. Instrum. Eng. **1220**, 46 (1990).
[15] H. C. Praddaude, D. W. Scudder, and B. Lax, Appl. Phys. Lett. **35**, 766 (1979).
[16] T. Lehner, Phys. Scr. **39**, 595 (1989).
[17] T. Lehner, Ph.D. thesis, L'Universite Pierre et Marie Curie, 1987.
[18] A. V. Nedospasov, Usp. Fiz. Nauk **94**, 439 (1968) [Sov. Phys. Usp. **11**, 174 (1968)].
[19] A. Garscadden, *Gaseous Electronics* (Academic, New York, 1978), Vol. 1, Chap. 2.
[20] E. A. Williams, D. Lininger, and M. Goldman, Phys. Fluids B Lett. **1**, 1561 (1989).
[21] H. R. Griem, *Plasma Spectroscopy* (Academic, New York, 1966).
[22] C. Clayton, C. Darrow, and C. Joshi, Appl. Opt. **24**, 2823 (1985).
[23] R. K. Jain and M. B. Klein, Appl. Phys. Lett. **35**, 454 (1979).
[24] R. K. Jain and D. G. Steel, Appl. Phys. Lett. **37**, 1 (1980).
[25] M. A. Khan, R. L. H. Bennet, and P. W. Kruse, Opt. Lett. **6**, 560 (1981).
[26] D. E. Watkins, J. C. R. Phipps, and S. J. Thomas, Opt. Lett. **6**, 76 (1981).
[27] W. P. Allis, Physica B+C **82C**, 43 (1976).
[28] L. Pekarek, Usp. Fiz. Nauk. **94**, 463 (1968) [Sov. Phys. Usp. **11**, 188 (1968)].
[29] K. W. Gentle, Phys. Fluids **9**, 2203 (1966).
[30] A. F. Nastoyashcii, Kvantovaya Elektron. (Moscow) **8**, 220 (1981) [Sov. J. Quantum Electron. **11**, 133 (1981)].
[31] A. F. Nastoyashchii, Fiz. Plazmy **3**, 752 (1977) [Sov. J. Plasma Phys. **3**, 425 (1977)].
[32] V. V. Breev, L. A. Knizhnikova, and A. F. Nastoyashchii, Fiz. Plazmy **9**, 1309 (1983) [Sov. J. Plasma Phys. **9**, 756 (1983)].
[33] R. W. P. McWhirter, *Plasma Diagnostic Techniques* (Academic, New York, 1965), Chap. 5.
[34] B. Y. Zel'dovich and P. Y. Raizer, *Physics of Shock Waves and High-Temperature Hydrodynamic Phenomena* (Academic, New York, 1966).
[35] A. B. Stewart, J. Appl. Phys. **27**, 911 (1956).
[36] Note that although the beat-wave equations are a linearization of the equilibrium equations, the beat-wave equations are still referred to as second-order equations in the expansion of the EM field amplitude.
[37] In the definition of ν_{hf}, we have combined some of the factors to form the Braginskii fluid electron-ion collision frequency.
[38] J. L. Spitzer, *Physics of Fully Ionized Gases* (Interscience, New York, 1956).

[39] M. Mitchner and J. Charles H. Kruger, *Partially Ionized Gases* (Wiley, New York, 1973).

[40] J. H. Ingold, *Gaseous Electronics* (Academic, New York, 1978), Vol. 1, Chap. 2.

[41] As noted in Sec. II, the constants c_3, c_4, etc. have been approximated as unity. References [39, 44] give the correct values. However, for our purposes, the approximated values are adequate.

[42] B. I. Davydov, Zh. Eksp. Teor. Fiz. **7**, 1064 (1937).

[43] T. Katsouleas, J. M. Dawson, and W. B. Mori, Bull. Am. Phys. Soc. **33**, 1991 (1988).

[44] S. I. Braginskii, *Transport Processes in a Plasma* (Consultants Bureau, New York, 1965), p. 205.

[45] B. Chapman, *Glow Discharge Processes* (Wiley, New York, 1980).

[46] S. C. Brown, *Basic Data of Plasma Physics* (MIT, Cambridge, MA, 1966).

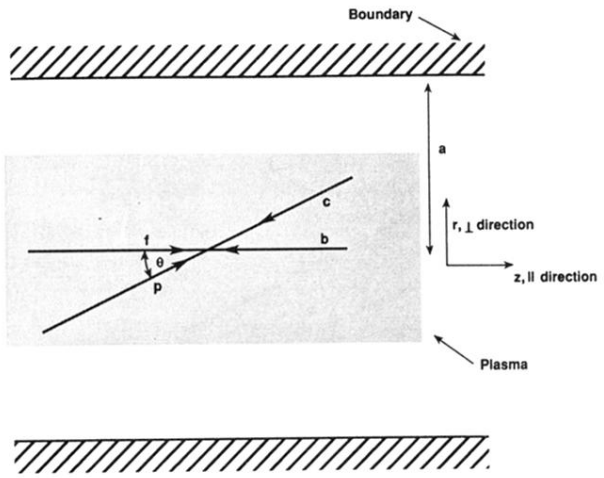

FIG. 2. FWM and plasma geometry for FWM in partially ionized plasma.

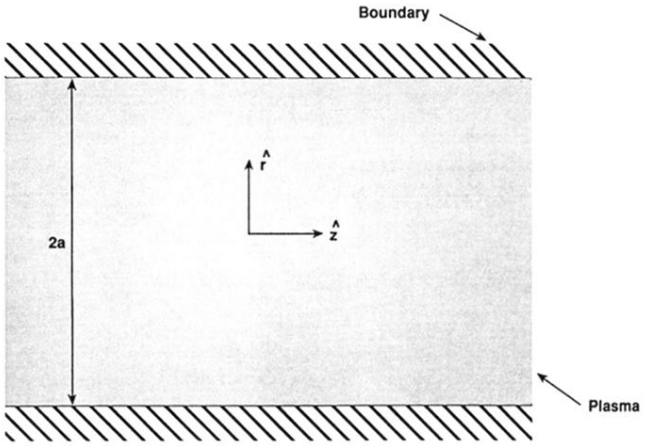

FIG. 8. Geometry for stability analysis of weakly ionized plasma.